Dept. of Math. University of Oslo
Statistical Research Report No. 2
ISSN 0806–3842 January 2007

MULTISEGMENT PRODUCTION PROFILE MODELS, A HYBRID SYSTEM APPROACH

Arne Bang Huseby and Nils F. Haavardsson
University of Oslo

Abstract

When an oil or gas field development project is evaluated, having a satisfactory production model is very important. Since the first attempts in the 40's, many different models have been developed for this purpose. Such a model typically incorporates knowledge about the geological properties of the reservoir. When such models are used in a total value chain analysis, however, also economical and strategic factors need to be taken into account. In order to do this, flexible modeling tools are needed. In this paper we demonstrate how this can be done using hybrid system models. In such models the production is modeled by ordinary differential equations representing both the reservoir dynamics as well as strategic control variables. The approach also allows us to break the production model into a sequence of segments. Thus, we can easily represent various discrete events affecting the production in different ways. The modeling framework is very flexible making it possible to obtain realistic approximations to real-life production profiles. At the same time the calculations can be done very efficiently. The framework can be incorporated in a full scale project uncertainty analysis.

1 Introduction

Models for estimating reserves and predicting production in oil and gas reservoirs have been studied extensively over many years. Many different models and methods have been suggested. A popular technique is the decline curve analysis approach. This approach dates back to the pioneer paper by [1] where the *exponential*, *hyperbolic* and *harmonic* curves were introduced. We will refer to these decline functions as the *Arps curves*. More recent papers considers other types of decline curves, and attempt to model the relation between the parameters of the curves and geological quantities. See e.g., [7], [8], [9] and [12].

The purpose of the present paper is to develop production models that can be used in the broader context of a total value chain analysis. In such an analysis the reservoir geology may be described by structure models, sedimentary models and saturation models. Stochastic models, combined with reservoir simulation, are applied to estimate the quantitative measures Stock Tank Original Oil In Place, Original Gas In Place and the Recovery Factor of the reservoir. The geological models and the quantitative measures are crucial to assess the quality, nature and prevalence of the oil resources in the reservoir.

The knowledge gathered from sample drilling, seismic surveys and other analyses is assembled and quantified in a full-scale reservoir model. The performance of the reservoir is assessed using some reservoir simulation software. These tasks are executed by geologists, geophysicists, petroleum engineers and other specialists. The output from a full-scale reservoir simulation includes oil production profiles and important performance measures such as Gas-Oil Ratio and Water Cut. Production profiles for gas- and water production may be derived from these performance measures.

In the present paper, we will assume that the properties of the reservoirs described above have already been assessed. We will also assume that a full-scale reservoir simulation has been performed and that output from such a simulation is given. A flexible modeling environment will be developed where these assessments can be utilized. Thus, we will focus more on the mathematical and numerical aspects of the modeling. This environment is intended to be used in the context of a total value

chain analysis where economic and strategic factors are taken into account as well. We will focus on single phased production, i.e., oil production only. Triple phased production, where oil production, gas production and water production are modeled simultaneously, is left for future work.

Execution time performance is an important issue in total value chain analysis. Usually, a simulation in a reservoir simulator takes hours, or even days. In the context of a total value chain analysis, where uncertainty should be incorporated, such execution times are unacceptable. Optimization problems, which also require low simulation execution time, are also relevant in total value chain analysis. For a discussion of total value chain analysis, see [5].

The perspective of the present paper is early stage analysis, done before production data are present. In the presence of production data many related problems may be studied using history matching of production data, see e.g., [11]. These related problems will not be studied here.

The present paper presents three contributions to production profile modeling:

- Production profiles are modeled using a multisegment approach where the production profile is decomposed into a combination of decline curves, one for each segment. This enables a satisfactory fit to the output from the reservoir simulation.
- The production is modeled using ordinary differential equations representing both the reservoir dynamics as well as strategic and economic control variables. This representation enables us to incorporate various types of delay in production in the framework. At the same time the calculations can be done very efficiently, so that the execution time remains acceptable even when uncertainty is incorporated into the framework.
- In the proposed framework multiple production profiles are easily analyzed, and many optimization problems may be studied. In this paper we will study subfields that share a central process facility. Due to capacity constraints of the central process facility, the operator needs to prioritize the production of the subfields.

2 Basic production profile functions

We start out by reviewing the classical decline function approach developed by [1]. For all the following models we assume that the production starts at a given time t_0. We denote the production rate at time $t \geq t_0$ by $q(t)$, and the corresponding cumulative production function at time $t \geq t_0$, by $Q(t)$.

Hyperbolic decline curves

The *hyperbolic* decline curve with initial production rate $r_0 > 0$, scale parameter $D > 0$, and shape parameter $b \in (0, 1)$ has the following form:

$$q(t) = r_0[1 + bD(t - t_0)]^{-1/b}. \tag{2.1}$$

By integrating this function from t_0 to t we get the corresponding cumulative production function:

$$Q(t) = \int_{t_0}^{t} q(u)du = \frac{r_0}{D(1-b)}[1 - (1 + bD(t - t_0))^{1-1/b}]. \tag{2.2}$$

We observe that the integral (2.2) converges as $t \to \infty$. Thus, if the production is allowed to continue forever, the ultimate recovery volume is given by:

$$\lim_{t\to\infty} Q(t) = \frac{r_0}{D(1-b)}. \tag{2.3}$$

Normally, however, the production is stopped when the production rate reaches some suitable cut-off level, say $r_c < r_0$. We can find the point of time when this happens by solving the equation $q(t) = r_c$ with respect to t. The solution, denoted t_c, is given by the following formula:

$$t_c = t_0 + \frac{1}{Db}[(\frac{r_0}{r_c})^b - 1]. \tag{2.4}$$

By inserting t_c into (2.2), we get what we refer to as the *technical recoverable volume*, denoted by V_r:

$$V_r = Q(t_c) = \frac{r_0}{D(b-1)}[(\frac{r_0}{r_c})^{b-1} - 1] \tag{2.5}$$

Due to economical considerations, the actual recovered volume may be smaller than this number. In this setting, however, we focus only on technical recoverable volumes.

Exponential decline curves

By letting $b \to 0$ in (2.1) we get the *exponential* decline curve. This decline curve has the following form:

$$q(t) = r_0 \exp(-D(t - t_o)). \tag{2.6}$$

The corresponding cumulative production function is given by:

$$Q(t) = \int_{t_0}^{t} q(u)du = \frac{r_0}{D}[1 - \exp(-D(t - t_0))]. \tag{2.7}$$

As in the hyperbolic case, the integral (2.7) converges, and the ultimate recovery volume is given by:

$$\lim_{t\to\infty} Q(t) = \frac{r_0}{D}. \tag{2.8}$$

Given a technical cut-off rate $r_c < r_0$, we solve the equation $q(t) = r_c$ with respect to t. The solution in this case is given by the following formula:

$$t_c = t_0 + \frac{1}{D}\ln(\frac{r_0}{r_c}). \tag{2.9}$$

By inserting t_c into (2.7), we get the technical recoverable volume:

$$V_r = \frac{r_0 - r_c}{D}. \tag{2.10}$$

Harmonic decline curves

The other limiting case of (2.1) where $b = 1$ is called the *harmonic* decline curve. This curve has the following form:

$$q(t) = r_0[1 + D(t - t_0)]^{-1}, \tag{2.11}$$

and the corresponding cumulative production function is given by:

$$Q(t) = \int_{t_0}^{t} q(u)du = \frac{r_0}{D}\ln(1 + D(t - t_0)). \tag{2.12}$$

Note that the integral (2.12) does *not* converge as $t \to \infty$. Thus, in this case it does not make sense to calculate the ultimate recovery volume. However, given a technical cut-off rate $r_c < r_0$, we can still solve the equation $q(t) = r_c$ with respect to t. The solution in this case is given by the following formula:

$$t_c = t_0 + \frac{1}{D}[\frac{r_0}{r_c} - 1]. \tag{2.13}$$

By inserting t_c into (2.12), we get the technical recoverable volume:

$$V_r = \frac{r_0}{D}\ln(\frac{r_0}{r_c}), \tag{2.14}$$

In order to unify the different families of decline curves, it is convenient to introduce the following function:

$$\Psi(x, z) = \begin{cases} \frac{z^x - 1}{x} & \text{if } x \neq 0, \\ \ln(z) & \text{if } x = 0, \end{cases} \quad \text{for all } -\infty < x < \infty, \text{ and } z \geq 1. \tag{2.15}$$

It is easy to verify that Ψ is continuous in x for all $z \geq 1$. By using this function we can easily express both t_c and V_r for all the three types of Arps curves:

$$t_c = t_0 + \frac{1}{D}\Psi(b, \frac{r_0}{r_1}), \tag{2.16}$$

$$V_r = Q(t_c) = \frac{r_0}{D}\Psi(b-1, \frac{r_0}{r_1}). \tag{2.17}$$

3 Multisegmented production functions

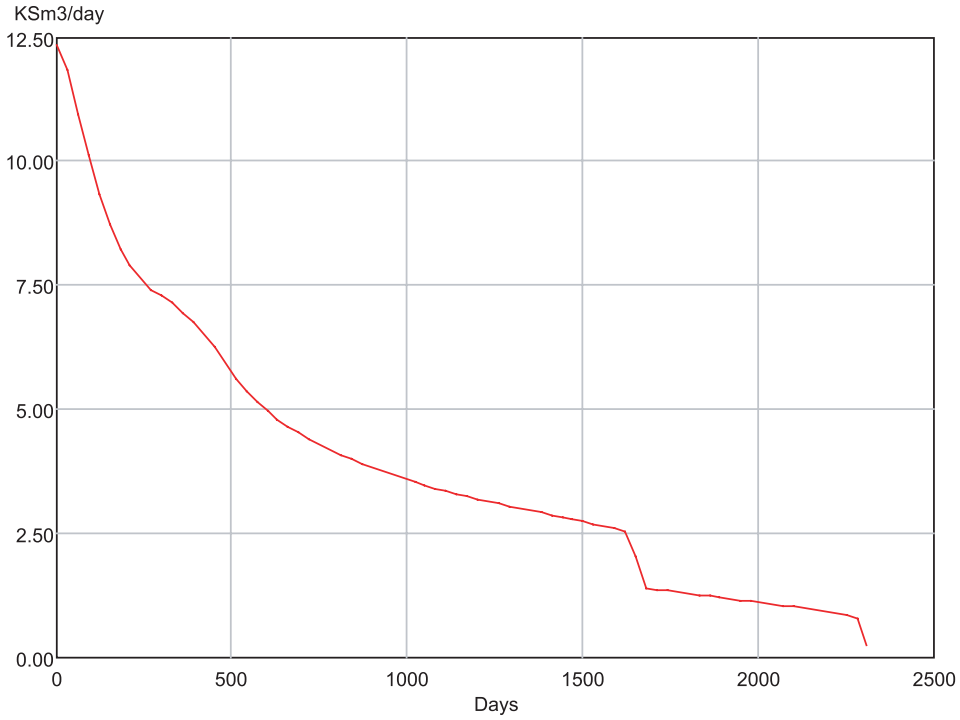

Figure 3.1: *Monthly production profile*

While the Arps decline curves covers a broad range of cases, these curves should be used with considerable caution. In many situations it may be necessary to use a combination of curves to get a satisfactory fit. The curve illustrated in Figure 3.1 shows an oil production profile from a real-life field. The curve was produced by using a full-scale reservoir model. As one can see, the curve consists of several clearly separated segments with quite different characteristics. In order to get an acceptable fit to this curve, the curve was divided into as many as 7 segments. For a similar discussion see [2].

In the following we assume that the production rate function is continuous and strictly decreasing. If this is not the case, the procedure needs to be modified slightly, but we skip these details here. The objective is to approximate the production function by using segments of Arps curves. Usually it is possible to do the segmentation of the curve simply by a visual inspection. We assume that this is done here, and that s segments will be used. Let $(t_0, r_0), (t_1, r_1), \ldots, (t_s, r_s)$ denote the locations of the segmentation points. Thus, the first segment runs between (t_0, r_0) and (t_1, r_1), the second segment runs between (t_1, r_1) and (t_2, r_2), etc. For each segment we calculate the volume produced within this segment. We denote these volumes by $V_1, \ldots, V_s$. Thus, we have:

$$V_i = \int_{t_{i-1}}^{t_i} q(t)dt, \text{ for } i = 1, \ldots, s. \tag{3.1}$$

In order to complete the curve fitting, we need to find scale parameters $D_1, \ldots, D_s$ and shape parameters $b_1, \ldots, b_s$ for the s segments. By applying (2.16) and (2.17), it follows that the parameters for the ith segment, i.e., D_i and b_i must satisfy the following two equations:

$$D_i = \frac{1}{t_i - t_{i-1}} \Psi(b_i, \frac{r_{i-1}}{r_i}), \tag{3.2}$$

$$D_i = \frac{r_{i-1}}{V_i} \Psi(b_i - 1, \frac{r_{i-1}}{r_i}). \tag{3.3}$$

Eliminating D_i from these equations, we get the following equation for b_i:

$$\frac{\Psi(b_i, \frac{r_{i-1}}{r_i})}{\Psi(b_i - 1, \frac{r_{i-1}}{r_i})} = \frac{r_{i-1}(t_i - t_{i-1})}{V_i}. \tag{3.4}$$

We first note that since we have assumed that the production function is strictly decreasing, it follows that $r_{i-1} > r_i$. From this it can be shown that the left-hand side of (3.4) is an increasing function of b_i. Moreover, we get that:

$$\lim_{b_i \to -\infty} \frac{\Psi(b_i, \frac{r_{i-1}}{r_i})}{\Psi(b_i - 1, \frac{r_{i-1}}{r_i})} = 1,$$

$$\lim_{b_i \to \infty} \frac{\Psi(b_i, \frac{r_{i-1}}{r_i})}{\Psi(b_i - 1, \frac{r_{i-1}}{r_i})} = \frac{r_{i-1}}{r_i}$$

Since the production function is strictly decreasing we also get that:

$$r_i(t_i - t_{i-1}) < V_i < r_{i-1}(t_i - t_{i-1}). \tag{3.5}$$

By using (3.5) on the right-hand side of (3.4), we get that:

$$1 < \frac{r_{i-1}(t_i - t_{i-1})}{V_i} < \frac{r_{i-1}}{r_i}. \tag{3.6}$$

Combining all this, we conclude that the equation (3.4) always has a unique solution. However, we are not guaranteed that the resulting b_i is a number between 0 and 1. If we insert $b_i = 0$ and $b_i = 1$ into the left-hand side of (3.4) we get the following restrictions on the right-hand side of (3.4):

$$\frac{\ln(\frac{r_{i-1}}{r_i})}{1 - \frac{r_i}{r_{i-1}}} \leq \frac{r_{i-1}(t_i - t_{i-1})}{V_i} \leq \frac{(\frac{r_{i-1}}{r_i}) - 1}{\ln(\frac{r_{i-1}}{r_i})}. \tag{3.7}$$

Given that (3.7) holds, a perfect fit can be found. If (3.7) does not hold, some sort of compromise is needed. If one insists on using curve segments of the Arps type, one could e.g., use the value of b_i within the interval $[0, 1]$ which is closest to the optimal solution. Thus, if the optimal value of b_i is negative, we replace this by 0, i.e., we use an exponential curve segment. If on the other hand the optimal value of b_i is greater than 1, we replace this by 1, i.e., we use a harmonic curve segment. In order to reduce the effect of using less than optimal shape parameters, one can use a finer segmentation. Alternatively, one may consider using other types of curve segments as well.

Finally, having found the shape parameters for each of the segments, the scale parameters can be calculated using either (3.2) or (3.3). Note, however, that if the optimal value of b_i is outside of the interval $[0, 1]$, we will get different numbers for the scale parameter depending on which of these equations we choose.

More specifically, if we calculate the scale parameter D_i using (3.2), the length of the interval of the curve segment will be $(t_i - t_{i-1})$. The volume under the curve segment, however, will not be equal to V_i. If the optimal $b_i < 0$, the resulting volume will be smaller than V_i, while if the optimal $b_i > 0$, the volume will be greater than V_i.

If, on the other hand, D_i is calculated using (3.3), the volume under the curve segment will be V_i. The length of the interval of the curve segment, however, will not be equal to $(t_i - t_{i-1})$. If the optimal $b_i < 0$, the resulting length of the interval will be longer than $(t_i - t_{i-1})$, while if the optimal $b_i > 0$, the length of the interval will be shorter than $(t_i - t_{i-1})$.

Ultimately, the choice of equation depends on which of the numbers, volumes or interval lengths, one considers to be most reliable. As a compromise, one could of course use both equations and let the scale parameter be the average of the two resulting numbers. For the rest of the paper, however, we have chosen to determine the scale parameters using (3.3). Note that this means that all the segment intervals must be adjusted after the shape parameters are fitted, and the corresponding scale parameters are calculated. More specifically, we keep the initial segmentation point, t_0, fixed, and adjust the other segmentation points recursively, using the following formula:

$$t_i = t_{i-1} + \frac{1}{D_i}\Psi(b_i, \frac{r_{i-1}}{r_i}), \qquad i = 1, \ldots, s. \tag{3.8}$$

Having fitted all the curve segments, we can calculate the resulting production rate function and cumulative production function. To do so, we introduce rate functions for the s segments, denoted $q_1, \ldots, q_s$ and given by:

$$q_i(t) = \begin{cases} r_{i-1}[1 + b_i D_i(t - t_{i-1})]^{-1/b_i}, & 0 < b_i < 1 \\ r_{i-1}\exp(-D_i(t - t_{i-1})), & b_i = 0 \\ r_{i-1}[1 + D_i(t - t_{i-1})]^{-1}, & b_i = 1. \end{cases} \quad \text{for all } t \in [t_{i-1}, t_i]. \tag{3.9}$$

We also introduce the cumulative production functions for the s segments, denoted $Q_1, \ldots, Q_s$ and given by:

$$Q_i(t) = \begin{cases} \frac{r_{i-1}}{D_i(1-b_i)}[1 - (1 + b_i D_i(t - t_{i-1}))^{1-1/b_i}], & 0 < b_i < 1 \\ \frac{r_{i-1}}{D_i}[1 - \exp(-D_i(t - t_{i-1}))], & b_i = 0 \\ \frac{r_{i-1}}{D_i}\ln(1 + D_i(t - t_{i-1})), & b_i = 1. \end{cases} \quad \text{for all } t \in [t_{i-1}, t_i]. \tag{3.10}$$

Using the above function the combined production rate function, denoted $q(t)$ as well as the combined cumulative production function can be calculated using the following formulas:

$$q(t) = \sum_{i=1}^{s} q_i(t)\,\mathrm{I}(t_{i-1} \le t \le t_i), \tag{3.11}$$

and:

$$Q(t) = \sum_{i=1}^{s} [Q_i(t)\,\mathrm{I}(t_{i-1} \le t \le t_i) + V_i\,\mathrm{I}(t > t_i)]. \tag{3.12}$$

Stochastic production profiles

So far we have assumed that the production profiles are known functions. In a risk analysis, however, one typically wants to include uncertainty into the model as well. In order to do so, one assesses probability distributions for all the uncertain quantities in the production model, and evaluate the risk by running a Monte Carlo simulation on the resulting stochastic model. In each iteration each of the uncertain quantities get values sampled from their respective distributions. Thus, the generated production functions may differ considerably from the one used in the curve fitting. In principle all the segment parameters (including even the number of segments) may be considered to be uncertain. Still it is often desirable to keep the overall shape of the function. This way we ensure that the simulated production functions behaves essentially like real-life functions. In the following discussion we assume that the number of segments, i.e., s and the shape parameters for the segments, i.e., $b_1, \ldots, b_s$ are kept constant during the simulations.

The main source of uncertainty is typically the segment volumes. Thus, to assess the production uncertainty, we start out by specifying a suitable joint distribution for $V_1, \ldots, V_s$. Given these volumes, we proceed to the next step by specifying a conditional joint distribution for the rates at the segmentation points, i.e., $r_0, r_1, \ldots, r_s$. Given all these quantities, the scale parameters $D_1, \ldots, D_s$ are found by (3.3). The point of time when the production starts, i.e., t_0 may be subject to uncertainty related to the progress of the development project, drilling activities etc. Thus, one will typically assess a separate uncertainty distribution for this quantity. The remaining segmentation points, however, i.e., $t_1, \ldots, t_s$, are calculated using (3.8). A Monte Carlo simulation of the production can then be done using the following procedure:

Algorithm 3.1 *For each simulation calculate the production rate function and the cumulative production using the following steps:*

STEP 1. *Generate $V_1, \ldots, V_s$ using the specified joint distribution.*

STEP 2. *Generate $r_0, r_1, \ldots, r_s$ using the specified conditional joint distribution.*

STEP 3. *Calculate $D_1, \ldots, D_s$ using* (3.3).

STEP 4. *Generate t_0, and calculate $t_1, \ldots, t_s$ using* (3.8).

STEP 5. *Calculate $q(t)$ and $Q(t)$ using* (3.11) *and* (3.12).

In the remainder of this section we propose a framework for modeling production uncertainty using the multisegmented production functions. We begin by considering volume uncertainty. To obtain reasonable results it is important to ensure that total reservoir volume, denoted by V gets a sensible distribution. Thus, it is often convenient to start out by assessing an uncertainty distribution for this volume. The segment volumes are then obtained as fractions of V. That is,

$$V_i = K_i \cdot V, \qquad i = 1, \ldots, s, \tag{3.13}$$

where $K_i = V_i/V$ denote the fraction associated with the ith segment, $i = 1, \ldots, s$. The joint distribution of $K_1, \ldots, K_s$ must be chosen so that $\Pr(\sum_{i=1}^{s} K_i = 1) = 1$. A simple way of constructing such a distribution is to start out with s independent nonnegative random variables, $\tilde{K}_1, \ldots, \tilde{K}_s$, and then obtain $K_1, \ldots, K_s$ by normalizing the $\tilde{K}_i$s so that their sum becomes 1. That is, we define:

$$K_i = \frac{\tilde{K}_i}{\sum_{j=1}^{s} \tilde{K}_j}, \qquad i = 1, \ldots, s, \tag{3.14}$$

This construction ensures that $\Pr(\sum_{i=1}^{s} K_i = 1) = 1$ regardless of the distributions of the $\tilde{K}_i$s. Thus, one has a large variety of distributions to choose from. In particular, it is well-known that if $\tilde{K}_i$ is Gamma distributed with shape parameter α_i and scale parameter β, for $i = 1, \ldots, s$, the resulting joint distribution of $K_1, \ldots, K_s$ is a Dirichlet distribution with parameters $\alpha_1, \ldots, \alpha_s$. For more on this see e.g., [4].

Alternatively, one can use a recursive approach where each segment volume is defined as a fraction of the remaining volume. That is, let $B_1, \ldots, B_{s-1}$ be $s-1$ independent random fractions, i.e., random variables with values in $[0, 1]$. For convenience we also introduce $B_s = 1$ reflecting that the last segment volume should always be equal to the remaining volume when all the other segment volumes are subtracted from V. We can then define the segment volumes recursively as follows:

$$V_i = B_i \cdot (V - \sum_{j=1}^{i-1} V_j), \qquad i = 1, \ldots, s. \tag{3.15}$$

By expanding the recursive formula the following alternative nonrecursive formula can be obtained:

$$V_i = B_i \prod_{j=1}^{i-1} (1 - B_j) \cdot V, \qquad i = 1, \ldots, s. \tag{3.16}$$

By comparing (3.13) and (3.16) it follows that the relationship between the K_is and the B_is can be expressed as:

$$K_i = B_i \prod_{j=1}^{i-1}(1 - B_j), \qquad i = 1, \ldots, s. \tag{3.17}$$

Alternatively, by inserting (3.13) into (3.15) and solving for B_i we get the following inverse relation:

$$B_i = \frac{K_i}{1 - \sum_{j=1}^{i-1} K_j}, \qquad i = 1, \ldots, s. \tag{3.18}$$

Note that since $B_s = 1$, it follows that:

$$K_s = 1 - \sum_{j=1}^{s-1} K_j, \tag{3.19}$$

or equivalently that $\sum_{j=1}^{s} K_j = 1$ as before.

Assuming that B_i has a density f_i on $[0, 1]$, for $i = 1, \ldots, s-1$, the resulting joint density of $K_1, \ldots, K_{s-1}$, denoted $g(K_1, \ldots, K_{s-1})$, can be found using the standard change-of-variable formula. Noting that the Jacobian of the inverse transformation (3.18) is triangular, it follows that g is given by:

$$g(K_1, \ldots, K_{s-1}) = \prod_{i=1}^{s-1} f_i \left(\frac{K_i}{1 - \sum_{j=1}^{i-1} K_j} \right) \cdot \frac{1}{1 - \sum_{j=1}^{i-1} K_j}. \tag{3.20}$$

Assume in particular that B_i is Beta distributed with parameters α_i and β_i, $i = 1, \ldots, s-1$. Then it follows that:

$$g(K_1, \ldots, K_{s-1}) \propto \prod_{i=1}^{s-1} \left(\frac{K_i}{1 - \sum_{j=1}^{i-1} K_j} \right)^{\alpha_i - 1} \left(\frac{1 - \sum_{j=1}^{i} K_j}{1 - \sum_{j=1}^{i-1} K_j} \right)^{\beta_i - 1} \cdot \frac{1}{1 - \sum_{j=1}^{i-1} K_j}, \tag{3.21}$$

where the normalizing constant is the product of the standard Beta distribution normalizing constants. By rearranging the terms it is easy to see that (3.21) can be written as:

$$g(K_1, \ldots, K_{s-1}) \propto \left[\prod_{i=1}^{s-1} K_i^{\alpha_i - 1} \right] \cdot \left[\prod_{i=1}^{s-2} (1 - \sum_{j=1}^{i} K_j)^{\beta_i - (\alpha_{i+1} + \beta_{i+1})} \right] \cdot \left[1 - \sum_{j=1}^{s-1} K_j \right]^{\beta_{s-1} - 1}. \tag{3.22}$$

Inserting $K_s = 1 - \sum_{j=1}^{s-1} K_j$ and $\alpha_s = \beta_{s-1}$, the density becomes:

$$g(K_1, \ldots, K_s) \propto \left[\prod_{i=1}^{s} K_i^{\alpha_i - 1} \right] \cdot \left[\prod_{i=1}^{s-2} (1 - \sum_{j=1}^{i} K_j)^{\beta_i - (\alpha_{i+1} + \beta_{i+1})} \right]. \tag{3.23}$$

In particular if $\beta_i = \alpha_{i+1} + \beta_{i+1}, i = 1, \ldots, s-2$, we see that $K_1, \ldots, K_s$ once again becomes Dirichlet distributed with parameters $\alpha_1, \ldots, \alpha_s$. This special case is a well-known result as well. See [4] for more details. In the following, however, we will not impose these restrictions on the parameters of the Beta distributions and instead use the more general distribution given in (3.23).

We then turn to modeling production rate uncertainty, i.e., the joint distribution of $r_0, r_1, \ldots, r_s$. Since the production function is assumed to be strictly decreasing, this distribution must be chosen so that $r_0 > r_1 > \cdots > r_s$ with probability one. A simple way to accomplish this is to introduce random fractions $C_1, \ldots, C_s$ with values in $[0, 1]$, and use the following multiplicative model:

$$r_i = C_i \cdot r_{i-1}, \qquad i = 1, \ldots, s. \tag{3.24}$$

If $C_1, \ldots, C_s$ are independent, the r_is will form a discrete time Markov chain. In addition to this we need to specify a suitable distribution for r_0. In general it may also be of interest to incorporate some sort of (typically positive) dependence between the r_is and the segment volumes. In many cases, however, it may be sufficient to include dependence between V and r_0.

Examples

We close the section by illustrating the proposed models with a few examples. In order to show the effect of uncertainty, we start out with a purely deterministic case, and then add increasing levels of uncertainty. In all examples we consider a production function consisting of four segments. In Table 3.1 the parameters of the deterministic production function are listed. The volumes are specified in KSm^3, while the rates are in KSm^3/day. In Figure 3.2 the resulting production rate function is plotted.

Segment (i)	1	2	3	4
Volume (V_i)	3600.0	2200.0	1500.0	700.0
Initial rate (r_{i-1})	10.0	3.5	2.5	1.5
End rate (r_i)	3.5	2.5	1.5	0.8
Shape parameter (b_i)	0.0	0.5	0.5	1.0

Table 3.1: *Parameter values for the deterministic production function*

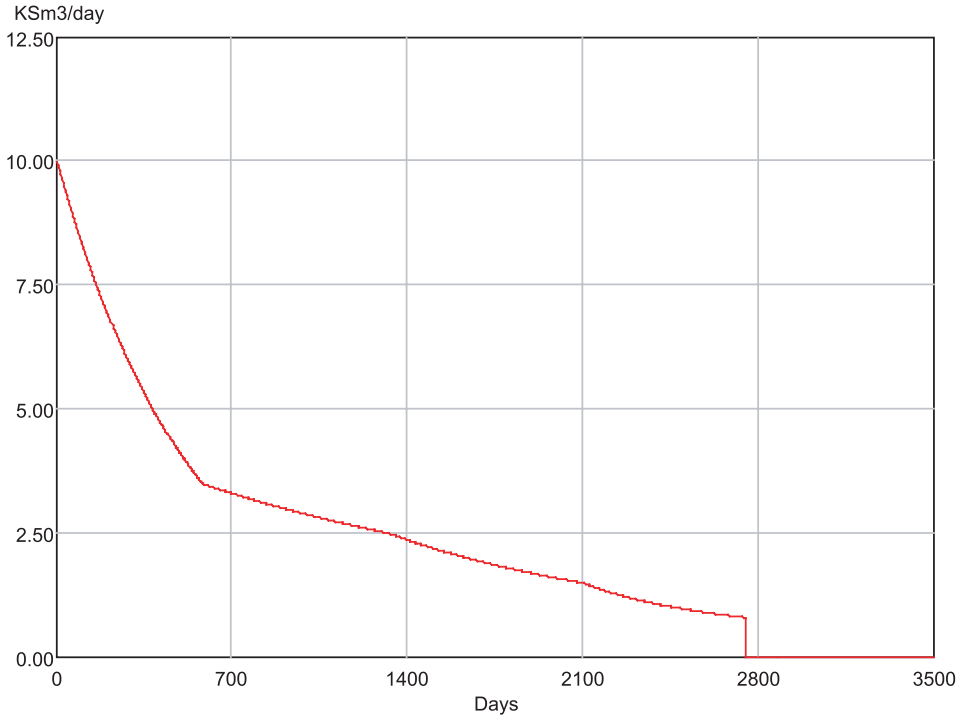

Figure 3.2: *Deterministic production rate function*

We then introduce uncertainty about the total volume, V and the initial production rate, r_0. As a joint distribution for V and r_0 we have chosen a bivariate lognormal distribution with $\text{Corr}(\ln(V), \ln(r_0)) = 0.7$. The means and standard deviations of this distribution are listed in Table 3.2.

	Mean	St.dev.
Total volume (V)	8000.0	1600.0
Initial rate (r_0)	10.0	2.0

Table 3.2: *Parameter values for the stochastic volume, V, and initial rate, r_0*

At this stage we do not include uncertainty about the volume and rate fractions. Instead we just

let these fractions be the same as in the deterministic model. That is, we let:

$$B_i = \frac{V_i}{\sum_{j=i}^{4} V_j}, \qquad i = 1, \ldots, 4, \tag{3.25}$$

and:

$$C_i = r_i / r_{i-1}, \qquad i = 1, \ldots, 4, \tag{3.26}$$

where $V_1, \ldots, V_4$ and $r_0, r_1, \ldots, r_s$ are given in Table 3.1. The resulting fractions are listed in Table 3.3. In Figure 3.3 we have plotted five different realizations of resulting production rate function. We observe that the shapes of the three curves are similar to the deterministic curve. The uncertainty, however, affects both the initial rate and the total volume under the curve. Thus, the resulting curves are not parallel to each other.

Segment (i)	1	2	3	4
Volume fractions (B_i)	0.450	0.500	0.682	1.000
Rate fractions (C_i)	0.350	0.714	0.600	0.533

Table 3.3: *Volume and rate fractions*

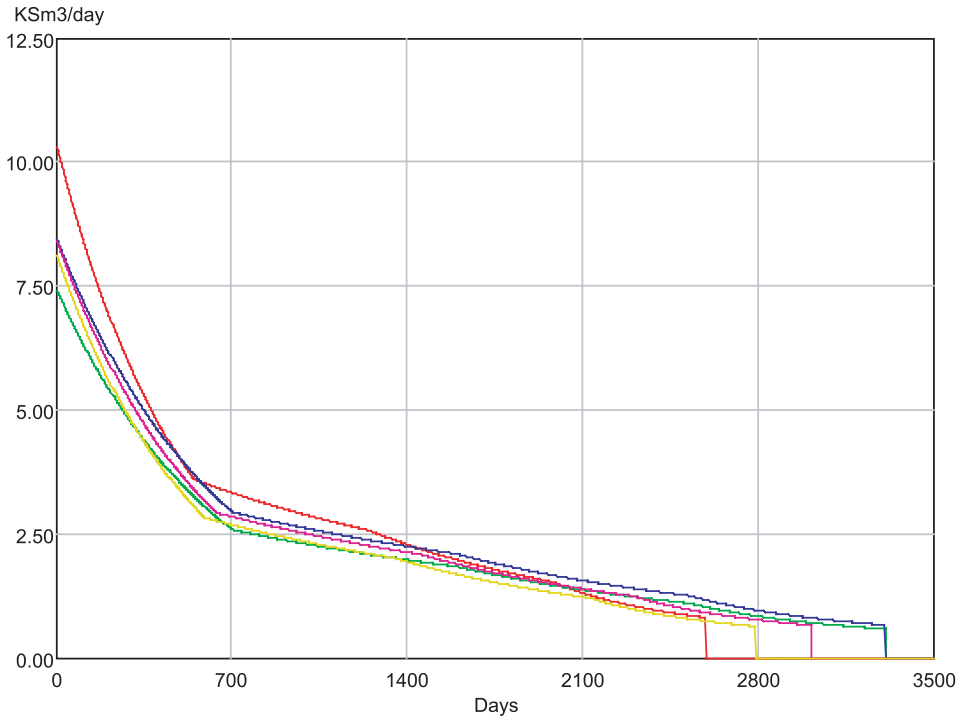

Figure 3.3: *Five realizations of the production profile with stochastic V and r_0*

In the final example we introduce uncertainty about the volume and rate fractions as well. For all fractions we use beta distributions. As mean values for these distributions we use the corresponding fractions in the previous model, while the standard deviations are set to 0.1. In Figure 3.4 we have plotted five different realizations of resulting production rate function. We observe that the shapes of the three curves are still similar to the deterministic curve. However, the curves vary much more than in the previous example.

Using Algorithm 3.1 we also ran 5000 simulations on the two uncertainty models, and calculated means and standard deviations for each point on the production rate functions and cumulative

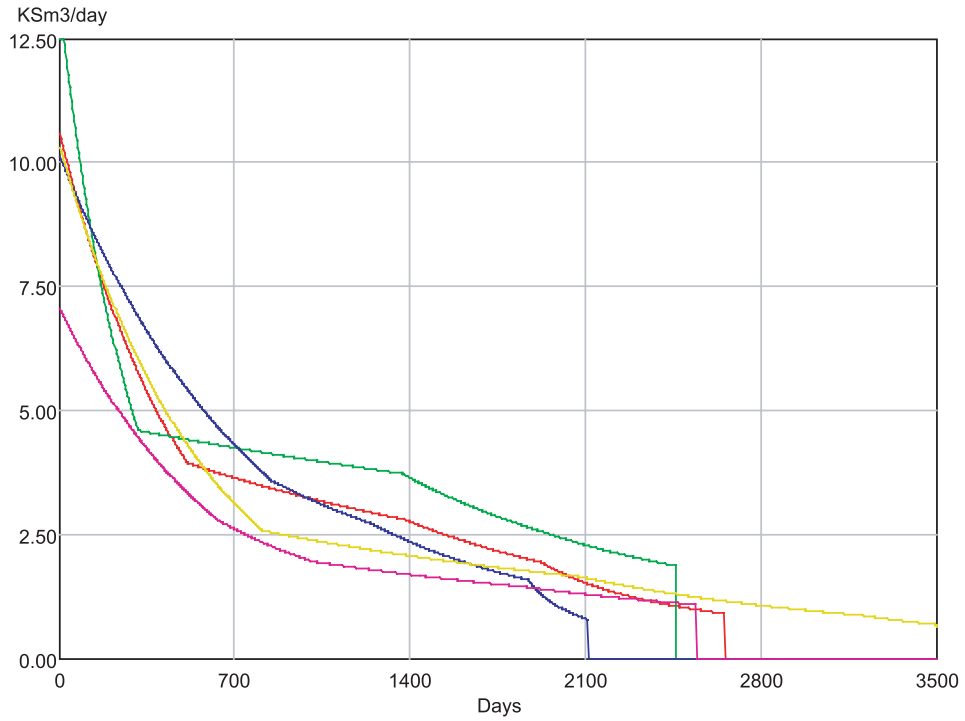

Figure 3.4: *Five realizations of the production profile with stochastic V, r_0 and stochastic volume and rate fractions*

production functions. Using these numbers we calculated upper and lower bounds for the rates and the cumulative values. As upper and lower bounds we used respectively the mean value plus and minus the standard deviation.

In Figure 3.5 and Figure 3.6 we have plotted the deterministic production rate and cumulative production together with the two corresponding sets of upper and lower bounds. The deterministic curves lies between the upper and the lower curves. The segmentation points are clearly visible on the deterministic production rate curve, while on the other curves these points have been smoothen out.

Since both the stochastic models use the same uncertainty distribution for the initial rate, r_0, the two sets of upper and lower bounds on the production rates start out in the same points. As the fraction uncertainties come into play, however, the interval between the upper and lower bound is larger for the fully stochastic model than for the model without fraction uncertainty.

Similarly, since both stochastic models use the uncertainty distribution for the total Volume, V, the upper and lower bounds on the cumulative curves converges to the same values as the time increases. The interval between the upper and lower bound is generally larger for the fully stochastic model than for the model without fraction uncertainty. However, the upper bounds appears to cross each other.

4 Production profiles as differential equations

In the previous sections we started out by fitting the production rate function, and then used this as the basis for calculating the cumulative production function. Since the Arps functions are easy to handle analytically, all the necessary calculations can be done very efficiently using explicit integration formulas like (3.12). This is especially convenient when the production model is part of a Monte Carlo simulation model. As demonstrated in the previous section it is easy to incorporate reservoir uncertainty into the model, and still keep the overall structure.

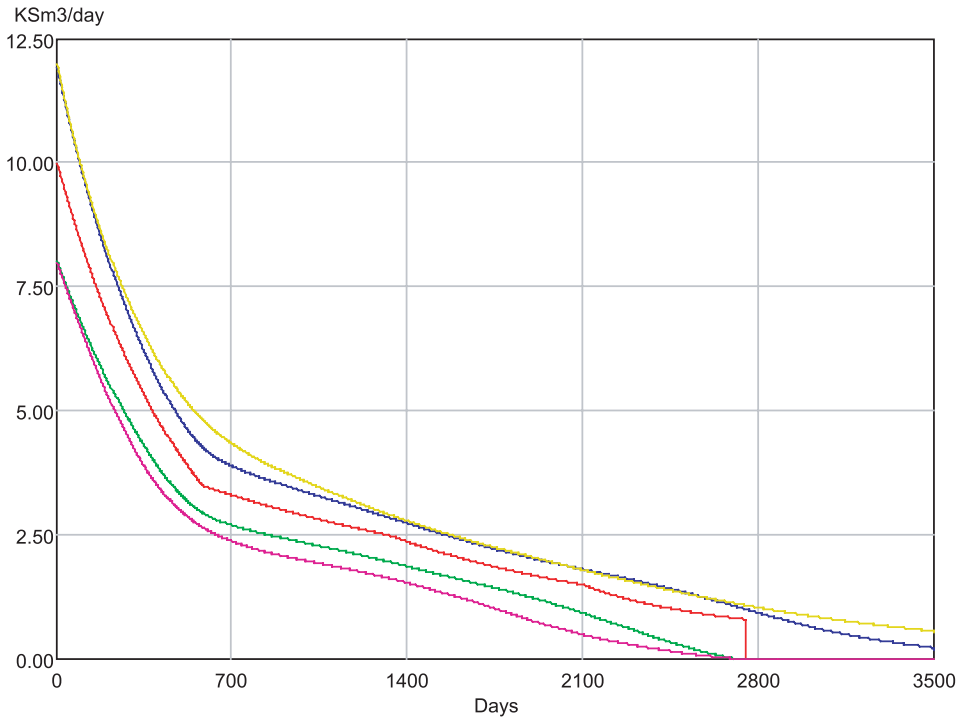

Figure 3.5: *Deterministic production rate (red curve), upper and lower bounds corresponding to the first stochastic model (blue and green curves) and the second stochastic model (yellow and purple curves)*

In many cases, however, this approach becomes too static. Having a production model with a fixed number of segments, makes it difficult to incorporate various types of production constraints, random irregularities in the flow, maintenance operations etc. An important observation here is that such external factors typically affect the short term production rate, but not the ultimate recoverable volume. Thus, if say, a well has to be shut down temporarily for maintenance, the total volume produced from this well may still be the same. The consequence of the operation is that the production is *delayed*. In order to incorporate external factors into the model, we need to include both the short term effect of the reduced production rate due to the maintenance operation, as well as the long term effect of the delayed production. In principle it is possible to model such effects by modifying the production rate function. However, it turns out to be far easier to do this by establishing a feed-back loop between the production rate and the cumulative production. That is, instead of modeling a simple one-way causal relation from the production rate to the cumulative production, we model the dynamic two-way relation between these two functions in terms of a differential equation. We will do this in two steps. In the first step we model the *internal* relation between the production rate and the cumulative production assuming no external factors, while in the second step we modify the internal relation by including external effects.

In general one can argue that the internal relation between the production rate and the cumulative production is essentially *time independent*, except for the fact that we need to specify when the production starts. Thus, if t_0 denotes the point of time when the production starts, the relation between the production rate function, q, and the cumulative production function, Q, should be of the following form:

$$q(t) = f(Q(t)), \qquad \text{for all } t \geq t_0, \tag{4.1}$$

with $Q(t_0) = 0$ as a boundary condition. Provided that the function f satisfies the well-known *Lipschitz condition*, there exists a unique solution to (4.1). See e.g., [3] for details about this. A differential equation of the form given in (4.1), where the function f depends only on Q, is called a

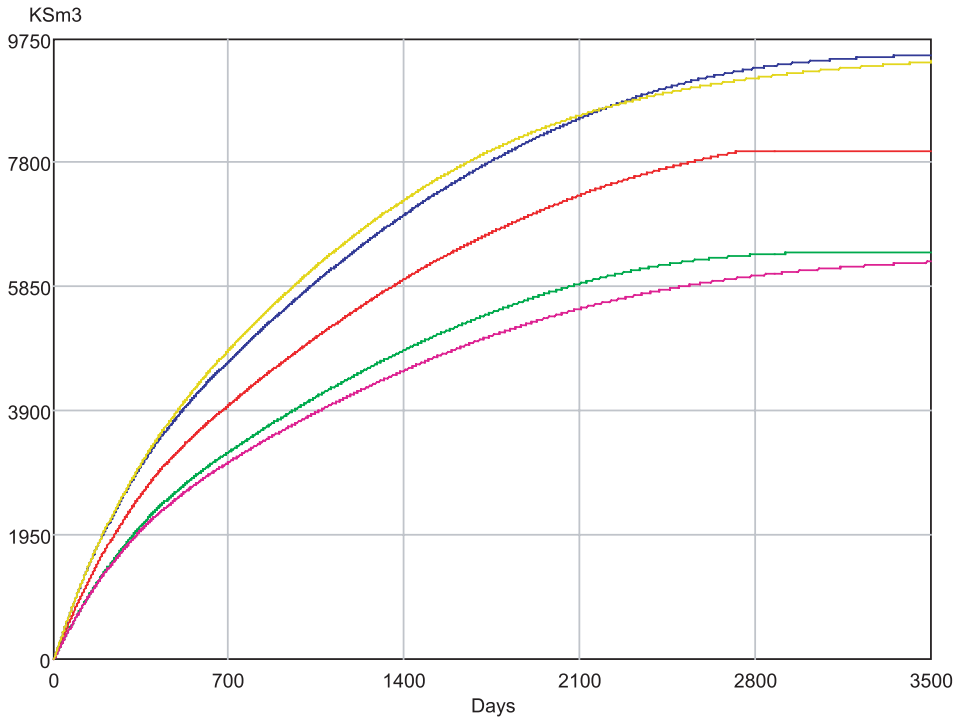

Figure 3.6: *Deterministic cumulative production (red curve), upper and lower bounds corresponding to the first stochastic model (blue and green curves) and the second stochastic model (yellow and purple curves)*

first order *autonomous* differential equation. Using standard numerical differential equation solvers, like e.g., Runge-Kutta's 4th order method, it is very easy to calculate the resulting production rate and cumulative production regardless of the function f. For details see e.g., [6]. Thus, this formulation allows us to work with many different functions. However, since the reservoir pressure falls as the reservoir is emptied, the function f will typically be a decreasing function.

The Li-Horne model

As a first example we consider the following differential equation introduced in [7]. We will refer to this as the *Li-Horne model*.

$$q(t) = a\frac{1}{Q(t)} - b. \tag{4.2}$$

Note that with the boundary condition $Q(t_0) = 0$, $q(t_0)$ is undefined. To avoid this problem, we assume that $Q(t_0) > 0$. It can be shown that this equation has the following unique solution:

$$\frac{\frac{a}{b} - Q(t)}{\frac{a}{b} - Q(t_0)} \exp(\frac{b}{a}(Q(t) - Q(t_0))) = \exp(-\frac{b^2}{a}(t - t_0)). \tag{4.3}$$

A proof of this is given in the Appendix. By letting $t \to \infty$ the righthand side of (4.3) becomes zero. Solving the resulting equation with respect to Q, shows that the ultimate recovery volume, $Q(\infty)$, is a/b.

We observe the expression (4.3) is valid also when $t_0 = Q(t_0) = 0$, in which case the expression becomes:

$$(\frac{a}{b} - Q(t)) \exp(\frac{b}{a}Q(t)) = \frac{a}{b} \exp(-\frac{b^2}{a}t). \tag{4.4}$$

Moreover, by differentiating (4.4), is easy to verify that $q(t) = a/Q(t) - b$ for all $t > 0$ in this case as well.

Finally, in the case, where $a = b = 1$, (4.4) becomes:

$$(1 - y)\exp(y) = \exp(-t), \tag{4.5}$$

which is the formula presented in [7].

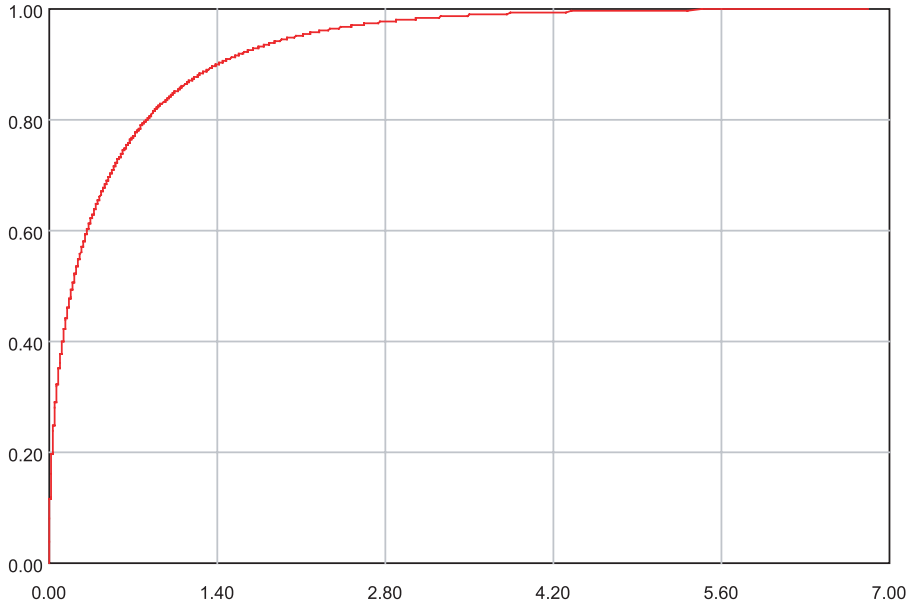

Figure 4.1: *Li-Horne Cumulative Production*

In Figures 4.1, and 4.2 we have plotted the cumulative production function and the production rate function for the Li-Horne model. We observe that production rate decreases very rapidly in the beginning, and the flattens out. In [7] this function is used to model oil production in core samples by spontaneous water imbibition. They also manage to link the constants a and b to specific properties of the reservoir.

Differential equations for the Arps curves

We will now try to connect the differential equation approach to the Arps functions and the fitting techniques discussed in the previous sections of this paper. Fortunately, it turns out that all the Arps functions can easily be formulated as autonomous differential equations.

As in the previous sections we start out by considering the hyperbolic function. That is, let $q(t)$ be given by (2.1), and let $Q(t)$ be given by (2.2). By rearranging the expression for Q, this can be written as:

$$[1 - \frac{D(1-b)}{r_0}Q(t)] = [1 + bD(t - t_0)]^{1-1/b}. \tag{4.6}$$

By raising this equation to the power of $1/(1-b)$ and multiplying by r_0, the right-hand side becomes equal to $q(t)$. Hence, we get the following differential equation:

$$q(t) = r_0[1 - \frac{D(1-b)}{r_0}Q(t)]^{1/(1-b)}. \tag{4.7}$$

The differential equation can also be written in the following form:

$$q(t) = r_0(\frac{D(1-b)}{r_0})^{1/(1-b)}[\frac{r_0}{D(1-b)} - Q(t)]^{1/(1-b)}. \tag{4.8}$$

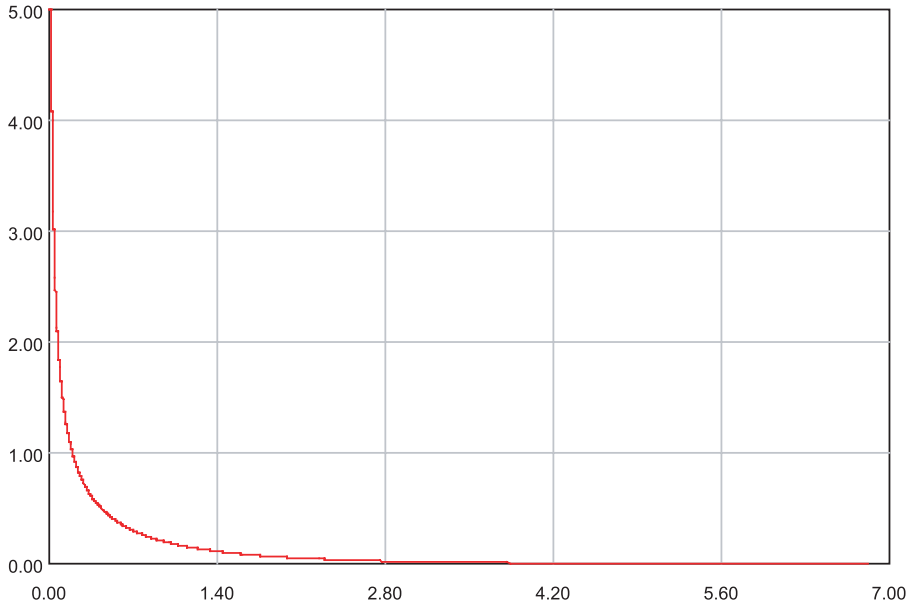

Figure 4.2: *Li-Horne Production Rate*

Recalling that by (2.3) the ultimate recoverable volume for this model is $r_0/(D(1-b))$, we see that the term $[r_0/(D(1-b)) - Q(t)]$ in (4.8) is equal to the remaining part of the ultimate recoverable volume at time t.

We then proceed in a similar fashion for the exponential function, in which $q(t)$ is given by (2.6) and $Q(t)$ is given by (2.7). By rearranging the expression for $Q(t)$ it is easy to see that we arrive the following differential equation:

$$q(t) = r_0[1 - \frac{D}{r_0}Q(t)], \tag{4.9}$$

which in fact also can be obtained directly as a special case of (4.7) by letting $b = 0$. The differential equation can also be written in a form analogous to (4.8) as follows:

$$q(t) = D[\frac{r_0}{D} - Q(t)], \tag{4.10}$$

where once again $[r_0/D - Q(t)]$ in (4.10) equals the remaining part of the ultimate recoverable volume at time t.

Finally, we turn to the harmonic function, where $q(t)$ and $Q(t)$ are given by (2.11) and (2.12) respectively. By applying the same technique as above it is easy to show that this model can be represented by the following differential equation:

$$q(t) = r_0 \exp(-\frac{DQ(t)}{r_0}). \tag{4.11}$$

Differential equations for multisegment profiles

The differential equation approach can also be extended to the more general situation where the production rate function consists of s segments. For each segment we assume that we have fitted a model in terms of a differential equation. As before we denote the production rate function and the

cumulative production function for the ith segment by q_i and Q_i respectively. Moreover, we assume that the relations between these functions are given by:

$$q_i(t) = f_i(Q_i(t)), \text{ for } i = 1, \ldots, s. \tag{4.12}$$

In order to connect these models, we need to specify a *switching rule* describing when to switch from one model to the next one. Such a switched system is a special case of so-called hybrid systems. For an introduction to switched systems, see e.g., [10]. One possible way to specify a switching rule, would be to calculate the switching points, $t_1, \ldots, t_s$ as we did in the previous section, and then switch from model to model as we pass these points. This is called a *time-dependent* switching rule. In this case, however, it turns out to be more convenient to use the *state* of the process, represented by the cumulative volume as a basis for the switching rule. This is called a *state-dependent* switching rule. As in the previous sections we denote the volumes produced in the s segments by $V_1, \ldots, V_s$ respectively. Moreover, the production rate function and the cumulative production function of the combined profile are denoted by q and Q respectively. The switching rule, $\sigma : \mathbb{R}^+ \to \{1, \ldots, s\}$ maps the state value, i.e., Q onto the corresponding segment index, and is given by the following:

$$\sigma(Q) = \begin{cases} 1 & \text{if } 0 \leq Q \leq V_1 \\ \ldots & \\ k & \text{if } \sum_{i=1}^{k-1} V_i < Q \leq \sum_{i=1}^{k} V_i \\ \ldots & \\ s & \text{if } \sum_{i=1}^{s-1} V_i < Q \leq \sum_{i=1}^{s} V_i \end{cases} \tag{4.13}$$

By using this switching rule, the combined differential equation can be written as:

$$q = f_{\sigma(Q)}(Q - \sum_{i<\sigma(Q)} V_i). \tag{4.14}$$

Modeling time dependent effects in production profiles

So far we have shown that all the models introduced in the previous sections, can be described equivalently in terms of differential equations. Still, in itself this reformulation does not simplify anything. In fact, it does not make much sense to use this approach at all whenever exact, explicit solutions, like those presented in the previous sections, are available. The main advantage with the differential equation approach, however, is that it allows us to model complex interactions between the pure production models and other models affecting the production in various ways, and still keep the physical relation between the production rate and the cumulative production intact. We will illustrate how this can be done, by considering a few examples.

Assume as above that we have fitted a production model in terms of a differential equation in the form (4.1). In the following we will refer to the function f as the *state-dependent* part of the production model. In a real-life situation there may be other things that affect the production rate as well. One such thing may be the production capacity. Capacity limitations are typically not functions of the production state, but rather functions of time. Thus, we let $c(t)$ denote the production capacity at time $t \geq t_0$. A model combining both the state-dependent part and the capacity limitation can then be written as:

$$q(t) = \min(c(t), f(Q(t))), \text{ for all } t \geq t_0. \tag{4.15}$$

The capacity function should of course always be nonnegative. Apart from that, however, in principle any measurable function can be used. As long as f satisfies the Lipschitz condition, so will the combined function. Normally, however, a typical capacity function would be a step function representing e.g., the combined production capacity from the available wells at a given point of time. Thus, each time a well is put in production, the capacity jumps up, while each time a well drops out, the capacity jumps down.

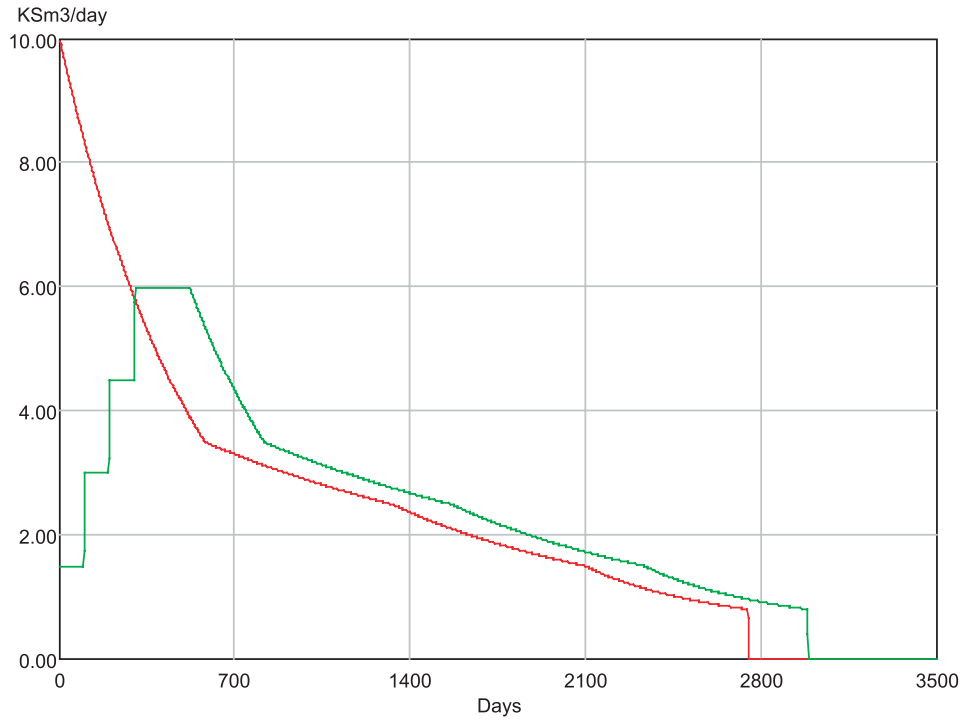

Figure 4.3: *Production rate with (green curve) and without (red curve) capacity limitations*

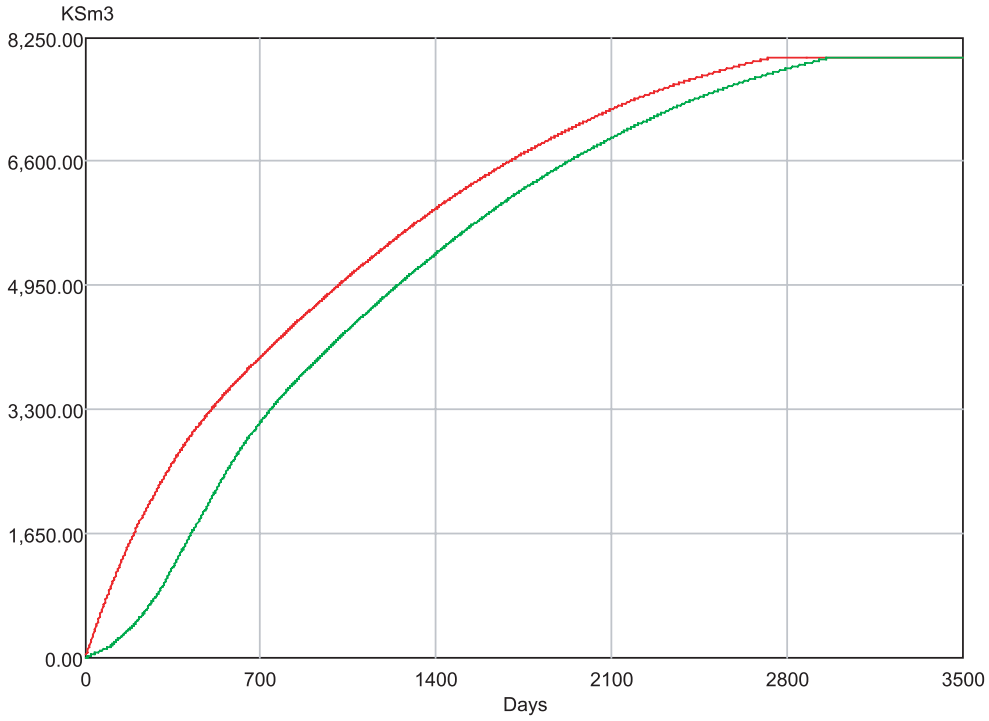

Figure 4.4: *Cumulative production with (green curve) and without (red curve) capacity limitations*

In the simplest cases the capacity function can be modeled as a deterministic step function. As

an example consider the deterministic production function with parameters listed in Table 3.1. We then combine this state-dependent function with a deterministic capacity function. The capacity function is partitioned into four segments. We consider a situation where the wells are put in production sequentially, and never drops out. The beginning of each segment corresponds to the point of time when a new well is put in production. Thus, the capacity values should form an increasing sequence. Moreover, the capacity values are assumed to be constant within each segment. The segment capacities (in KSm3) and durations (in Days) are listed in Table 4.1. The last segment of the c function is assumed to last throughout the remaining lifetime of the field, so for simplicity the duration of this segment is set to ∞.

Segment (i)	1	2	3	4
Capacities	1.5	3.0	4.5	6.0
Durations	100	100	100	∞

Table 4.1: *Segment capacities and durations*

We calculated the production rates and the cumulative production for the two models using a standard Runge-Kutta's 4th order differential equation solver. The results are plotted in Figure 4.3 and Figure 4.4. We observe that the two curves are quite different in the beginning when the c function is the dominating term of (4.15). As the state-dependent part becomes dominating, however, the two curves become identical except for a time lag. This lag occurs since the capacity constraints slows the production down in the early stages. This lag is seen in the cumulative curves as well. Still the two cumulative curves end up at the same point corresponding to the total volume of the field.

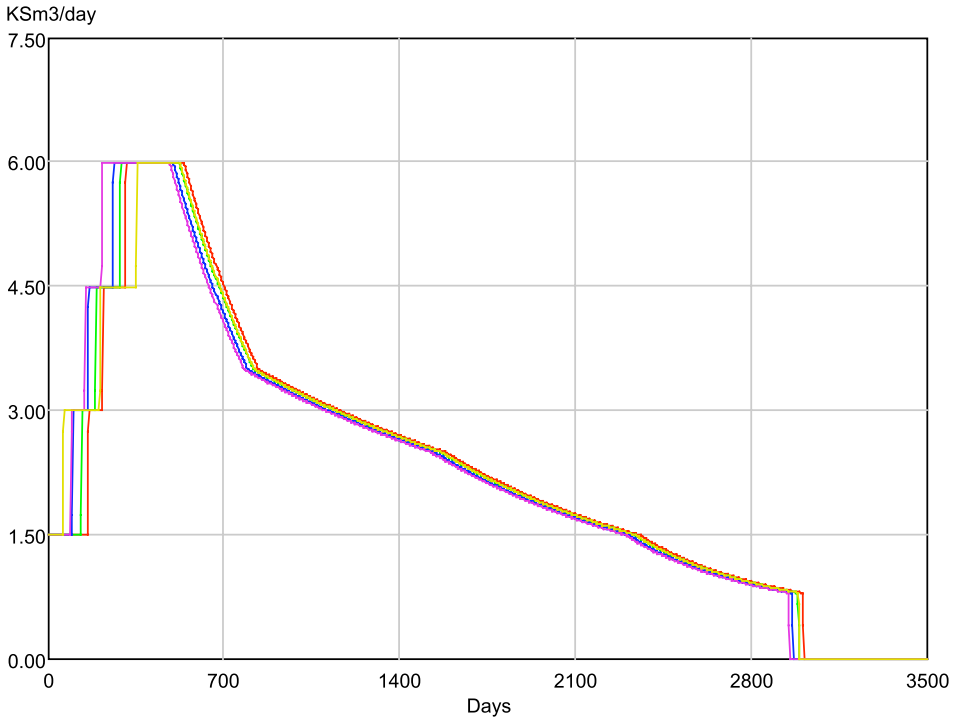

Figure 4.5: *Five realizations of the production profile with stochastic durations*

More generally, both the capacity part and the state-dependent part can be stochastic. In order to focus on the effect of a stochastic capacity, we keep the state-dependent part deterministic for now, and include only uncertainty about the capacity. More specifically we consider two cases. In the first case we let the durations of each segment be stochastic, while the capacity values are kept

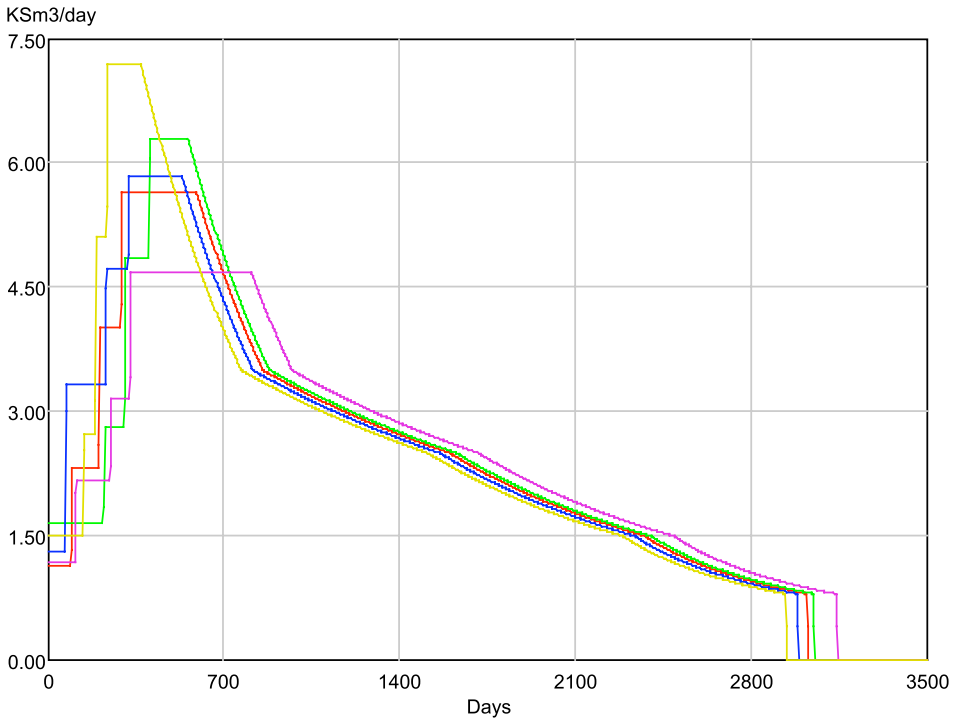

Figure 4.6: *Five realizations of the production profile with stochastic durations and capacity values*

constant. For simplicity the durations are assumed to be independent and lognormally distributed with means 100 and standard deviations 50. In Figure 4.5 we have plotted five different realizations of this model.

In the second case we also include uncertainty about the capacity values. To get an increasing sequence of capacity values for the four segments, we used a simple additive model, where the capacity at a given point of time is equal to a sum of independent stochastic variables, and where the number of terms in the sum is equal to the number of wells in production at that given point of time. All the terms where assumed to be lognormally distributed with means 1.5 and standard deviations 0.5. In Figure 4.6 we have plotted five different realizations of this model.

Comparing the two plots, we see that while all the curves in the first plot are just lagged versions of the same curve, the curves in the second plot are far more widespread. Still the later stages of the production profiles are not affected as much by the capacity uncertainty, which of course is no surprise.

Using Runge-Kutta's 4th order method we also ran 5000 simulations on the two uncertainty models, and calculated means and standard deviations for each point on the production rate functions and cumulative production functions. Using these numbers we calculated upper and lower bounds for the rates and the cumulative values. As in the previous section we used the mean value plus and minus the standard deviation as upper and lower bounds respectively.

In Figure 4.7 and Figure 4.8 we have plotted respectively the deterministic production rate and the cumulative production together with the two corresponding sets of upper and lower bounds. Compared to Figure 3.5 and Figure 3.6 we see that the effect of the capacity uncertainty is much less noticeable. In particular, the cumulative curves all converges to the same point, i.e., the fixed total volume.

As we have seen, the capacity function allows us to incorporate variable production constraints related to major changes in the operational settings, e.g., corresponding to wells being put in or out of production. However, when running an oil field, the production rate is also affected by short term irregularities. To include such phenomena into the production model, it is more natural to

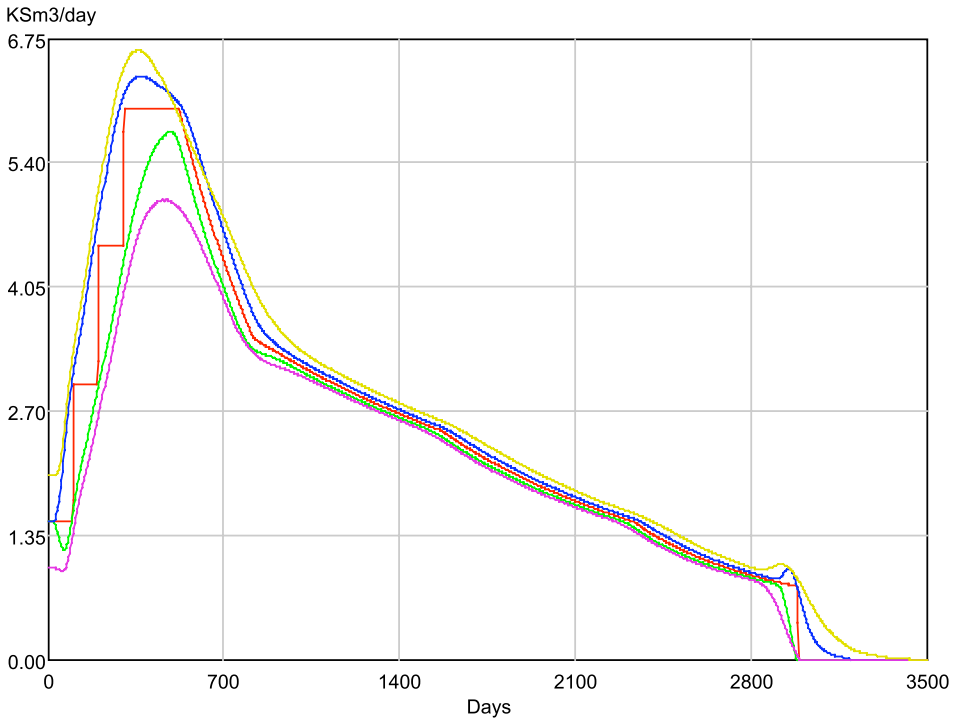

Figure 4.7: *Deterministic production rate (red curve), upper and lower bounds corresponding to the first stochastic model (blue and green curves) and the second stochastic model (yellow and purple curves)*

use a continuous time stochastic process. More specifically, we introduce a stochastic process $\{r(t)\}$ such that for any given point of time t, $r(t)$ represents the fraction of the production rate that is actually produced at this point of time. This process is referred to as the *regularity process*. When this process is incorporated into the model, the resulting differential equation becomes:

$$q(t) = r(t) \cdot \min(c(t), f(Q(t))), \text{ for all } t \geq t_0. \tag{4.16}$$

As long as $r(t)$ is measurable almost surely, we can easily extend our framework to cover this situation. Since $r(t)$ is supposed to be a fraction, a model for this process should be such that $\Pr(r(t) \in [0,1]) = 1$ for all t. In fact to get a realistic model, one should typically choose an even smaller interval for $r(t)$. As an example we consider a case where $r(t)$ is uniformly distributed on $[a,b]$ for each t, where $0 \leq a < b \leq 1$. In order to incorporate some time dependence into the model, $r(t)$ is obtained as a transformation of a Gaussian process. More specifically, let $\{U(t)\}$ be a gaussian process such that:

$$\begin{aligned} \mathrm{E}[U(t)] &= 0 \text{ for all } t \geq 0, \\ \mathrm{Cov}[U(s), U(t)] &= \rho^{|t-s|} \text{ for all } s, t \geq 0, \end{aligned}$$

where $\rho \in (-1, 1)$. Furthermore, let Φ denote the cumulative distribution function for the standard normal distribution. It is then easy to see that we can transform this process into the desired regularity process using the following formula:

$$r(t) = a + (b - a) \cdot \Phi(U(t)) \tag{4.17}$$

In order to compute the resulting stochastic production rate and cumulative production, we used a stochastic version of Runge-Kutta's 4th order method. The main adjustment to the standard

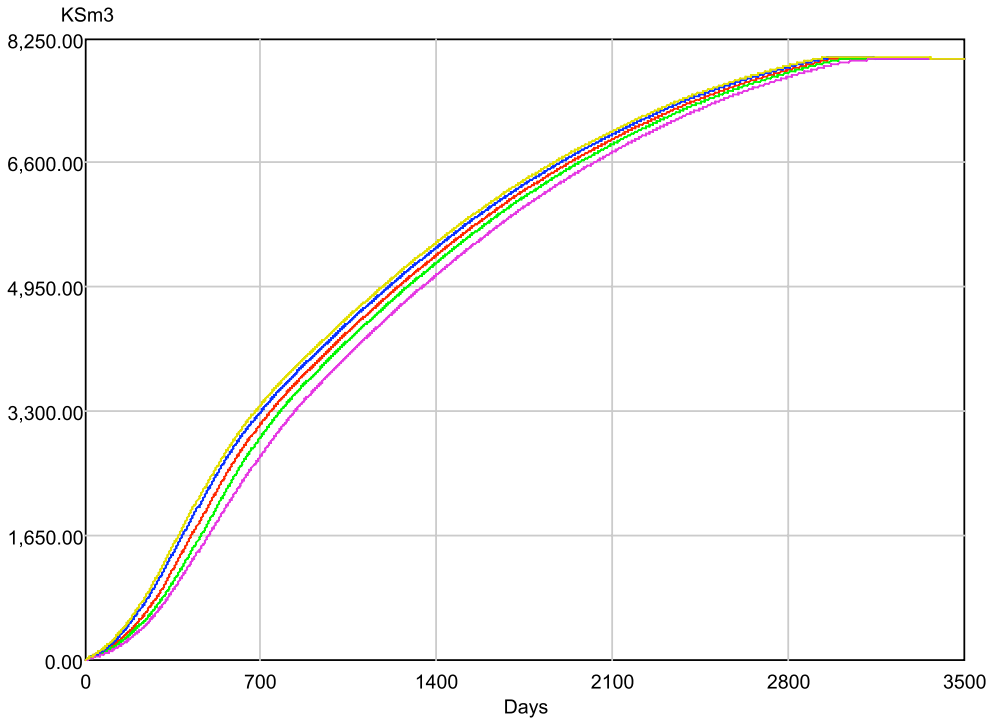

Figure 4.8: *Deterministic cumulative production (red curve), upper and lower bounds corresponding to the first stochastic model (blue and green curves) and the second stochastic model (yellow and purple curves)*

algorithm is that in order to get the correct time dependence, one must make sure that the $U(t)$-values are reused in the look-ahead steps.

As an example we consider a case where we use the same deterministic state-dependent function and capacity function as we did in our previous examples. The regularity process is modeled as described above with $a = 0.9$, $b = 1.0$ and $\rho = 0.8$. In Figure 4.9 we have plotted the resulting production rate together with the corresponding curve without the regularity process. By including $r(t)$ into the differential equation the resulting production rate becomes much more noisy. The long term effect of this is that the production is slowed down by 5% on average. Thus, the production is slightly delayed compared to the deterministic curve. In the cumulative curve the noise is evened out so the only visible effect of $r(t)$ is the production delay.

5 Multiple production profiles

In many cases it is of interest to model the production from several subfields simultaneously. Common capacity constraints are often imposed on subfields belonging to a larger field or group of fields. Such constraints may for example be the total capacity at a processing facility. We will now show how such a situation can be managed within our framework. More specifically, we assume that we have a field consisting of n subfields. The production from these subfields are processed on a common processing facility with a given processing capacity per unit of time.

We start out by modeling the *potential production* from each the subfields given no common capacity constraints. The potential production rate function for subfield i at time t is denoted by $q_i^{pot}(t)$ and is expressed as:

$$q_i^{pot}(t) = g_i(t, Q_i(t)), \ i = 1, \ldots, n, \tag{5.1}$$

where $Q_i(t)$ represents the cumulative production function of subfield i at time t, and g_i represents

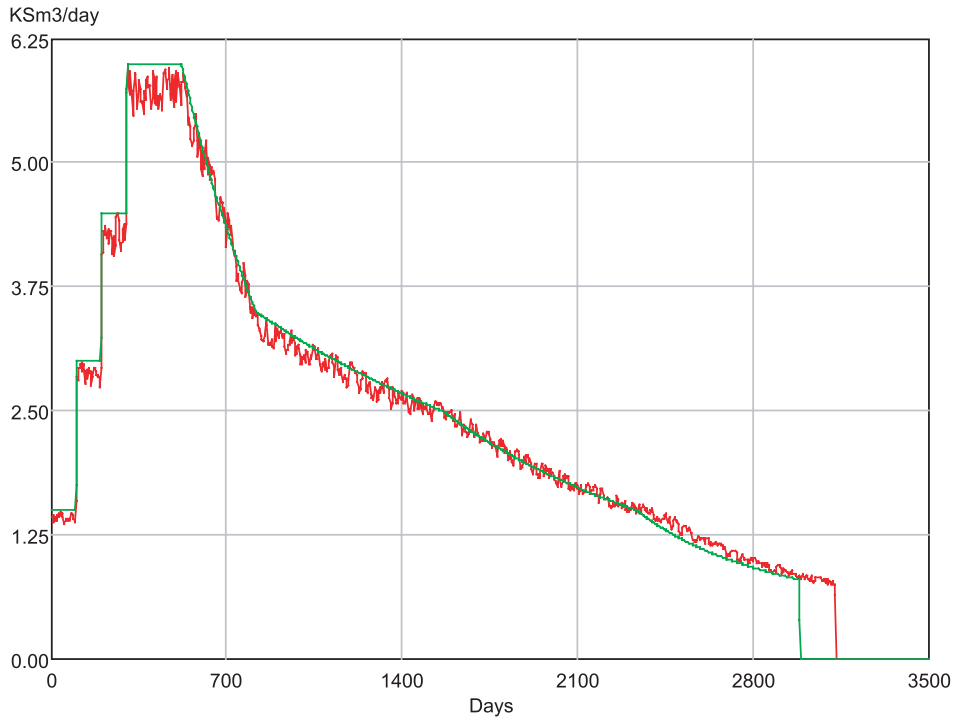

Figure 4.9: *Production rate with (red curve), and without (green curve) the regularity process*

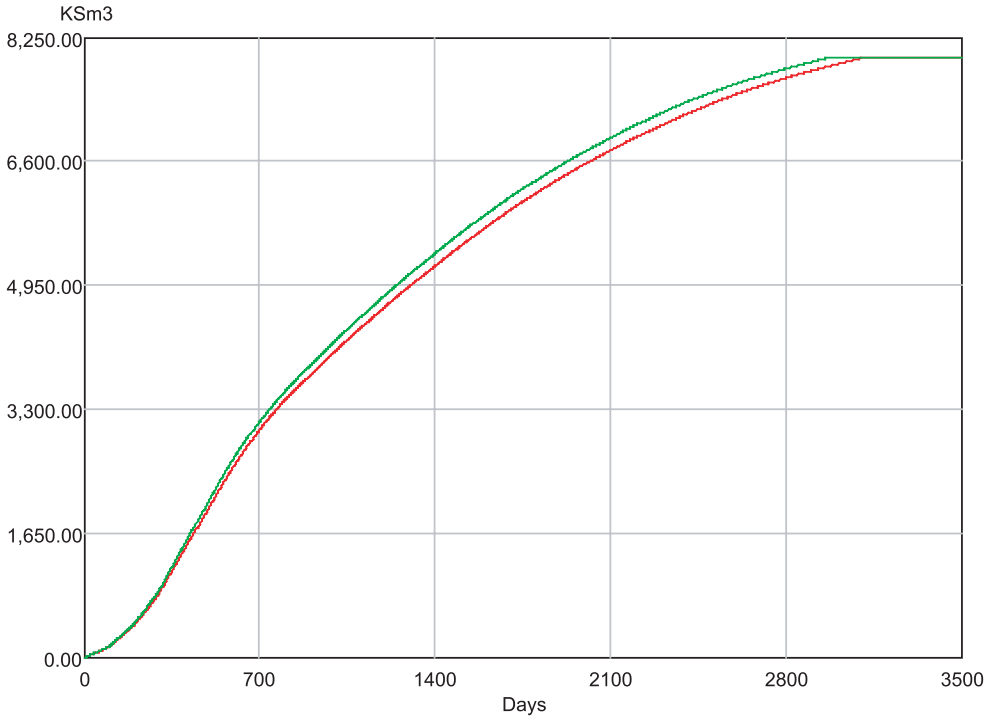

Figure 4.10: *Cumulative production with (red curve), and without (green curve) the regularity process*

both the time and state dependent parts of the model for subfield i. Thus, g_i may include segments,

time dependent subfield constraints and regularity as explained in the previous section.

The processing capacity at time t is denoted by $K(t)$. To ensure that the total production does not exceed $K(t)$, the production from each subfield has to be restricted in some way. This can be done by introducing *choke factors* for each of the subfields. Thus, let $a_i(t) \in [0,1]$ denote the choke factor for the ith subfield at time t, $i = 1, \ldots, n$. The resulting production from the ith subfield at time t is then given by $q_i(t) = a_i(t)q_i^{pot}(t)$, $i = 1, \ldots n$. In order to satisfy the processing constraint, the choke factors must be chosen so that:

$$\sum_{i=1}^{n} a_i(t)q_i^{pot}(t) \leq K(t) \text{ for all } t \geq 0. \tag{5.2}$$

Clearly there are an infinite number choices for the choke factors. Typically, one would be interested in finding choke factors that are optimal with respect to some suitable criterion. E.g., one could try to maximize the total discounted production from all the subfields. Solving such optimization problems can be difficult, especially when uncertainty is included in the model, so this is beyond the scope of the present paper. Instead we will present some possible ad. hoc. strategies for the choke factors.

The symmetric strategy. When using the symmetric strategy, the available process capacity is shared proportionally between the different fields. If the current production exceeds the process capacity of the central processing facility, the production of every field is scaled down with a common choke factor. That is, we let

$$a_i(t) = \frac{K(t)}{\sum_{j=1}^{n} q_j^{pot}(t)}, \; i = 1, \ldots, n, \tag{5.3}$$

where $K(t)$ denotes process capacity of the central processing facility.

The priority strategy. For this strategy the fields are prioritized initially according to some suitable criterion. Let $\boldsymbol{\pi} = (\pi(1), \ldots, \pi(n))$ be the permutation vector representing the order at which the fields are prioritized. That is, field number $\pi(1)$ is given the highest priority, field number $\pi(2)$ is given the second highest priority, etc. The choke factors are then defined as:

$$\begin{aligned}
a_{\pi(1)}(t) &= \min\{1, \frac{K(t)}{q_{\pi(1)}^{pot}(t)}\}, \\
a_{\pi(2)}(t) &= \min\{1, \frac{K(t) - a_{\pi(1)}(t)q_{\pi(1)}^{pot}(t)}{q_{\pi(2)}^{pot}(t)}\}\}, \\
&\ldots \\
a_{\pi(n)}(t) &= \min\{1, \frac{K(t) - \sum_{j=1}^{n-1} a_{\pi(j)}(t)q_{\pi(j)}^{pot}(t)}{q_{\pi(n)}^{pot}(t)}\}\}.
\end{aligned} \tag{5.4}$$

Note that if $q_{\pi(i)}^{pot}(t) = 0$ for some i and t, the corresponding choke factor is undefined in (5.4). To avoid this problem, we simply replace the corresponding choke factor by 1 in such cases.

The fixed maximal quota strategy. Sometimes it may not be possible to adjust the choke factors continuously. Instead one have to choose fixed maximal production rates for the subfields initially, and use the same values throughout the lifeime of the field. More specifically, assume that the ith subfield is given a fixed maximal quota κ_i for the entire production period, $i = 1, \ldots, n$. The resulting production from the ith subfield at time t is then given by $q_i(t) = \min\{\kappa_i, q_i^{pot}(t)\}$, $i = 1, \ldots n$. In order to satisfy the processing constraint, the quotas must be chosen so that:

$$\sum_{i=1}^{n} \kappa_i \leq K(t), \text{ for all } t \geq 0. \tag{5.5}$$

In particular, if $K(t) = K$ for all t the quotas should be chosen so that their sum is equal to K.

Regardless of which strategy one chooses for the choke factors, it is easy to run simulations on all the subfields simultaneously. The fact that we now have a set of n ordinary differential equations instead of just one, does not cause any problems. All the calculations can still be done using e.g., a standard Runge-Kutta's 4th order differential equation solver.

5.1 An example with different choices of production quota constraints

In this example we will study both continuous control constraints and quota model constraints. This case study is based on real reservoir simulation data from two actual fields. We assume that two fields share a central processing facility. In one of the fields water is injected into the reservoir to maintain reservoir pressure. We will refer to this field as the *maintenance field*. In the other field the reservoir is depleted without water being injected. This field is referred to as the *depletion field*. In most cases water or gas will be injected into the reservoir to maintain reservoir pressure if it is economically viable to do so. However, some times there are good reasons not to inject water or gas into the reservoir, for example if the field of interest is too small.

Table 5.1 summarizes the characteristics of the production rates of the two fields. The depletion field is described by a production rate curve with two segments, while the maintenance field has a production rate curve with four segments. Table 5.2 states the characteristics of the field capacities of the two fields. The capacity of the central processing facility is assumed to be 2500 Sm3/d in this example. Production is assumed to commence immediately in both fields. Finally, Table 5.3 states the regularity parameters selected in this example. Figure 5.1 illustrates the simulation profile and the matched profile comparison of the production rate for the depletion field and the maintenance field.

Figure 5.2 show the results of implementing three different choices of constraints in our prototype. Symmetry constraints are illustrated in the upper left panel in Figure 5.2 and priority constraints are illustrated in the upper right panel. The maintenance field is prioritized throughout the entire production period. As a contrast to these continuous control constraints we have also implemented a constant quota model. In such a model the quotas of each field is decided once and for all before the production commences. The lower panel in Figure 5.2 shows the results of an implementation of a constant quota model where the maintenance field receives a constant quota of 1800 Sm3/d while the depletion field receives a constant quota of 700 Sm3/d. As we can see from these three figures the production rates of the two fields are quite different depending on what constraints are being implemented.

An important issue is how our choice of constraints impacts the total cumulative production. The left panel in Figure 5.3 shows total cumulative production for the three choices of constraints. Since the fields will be emptied regardless of the choice of constraints, we are ultimately interested in selecting the constraints that maximizes the discounted production and the net present value. From Figure 5.3 we can see that the priority constraints yields the highest discounted production value. The constant quota model yields the poorest discounted production value, while the discounted production of the symmetry constraints is a little lower than the discounted production of the priority constraints.

The initial choice of quotas in the constant quota clearly has a tremendous impact on the discounted production. To optimize discounted production with respect to initial quotas we let the constant quotas of the maintenance field and the depletion field vary between 0 and 2500 which is the capacity of the central processing facility. The right panel in Figure 5.3 illustrates discounted production as a function of the constant quota assigned to the maintenance field. We can see from the right panel in Figure 5.3 that by assigning a quota of 2058 Sm3/d to the maintenance field and 442 Sm3/d to the depletion field the discounted production is maximized. In Table 5.4 the discounted production values are summarized for the different strategies. We can see that when the constant quota model is optimized with respect to constant quota, its discounted production is almost as high as the discounted production of the symmetry constraints. The priority constraints yields the highest discounted production regardless of whether the constant quota model is optimized.

To give some intuition on the economic values of the different choices, Table 5.5 summarizes the net present value of the different choices of constraints. The net present value is calculated using

an oil price of 55 USD per barrel of oil, which reflects the spot price level of Brent at the time the article is written. The oil price has fluctuated considerably in the past. Table 5.6 shows the difference in net present value in USD between the priority constraints and the quota constraints for some different choices of oil price.

Field	Segm. i	Start rate r_{i-1} (Sm3/d)	Stop rate r_i (Sm3/d)	Segm. vol. V_i (KSm3)	Shape param. b_i
Depletion	1	3995	1395	315.3	0.0
Depletion	2	1395	100	1182.5	0.8
Maintenance	1	9995	5525	993.2	0.0
Maintenance	2	5525	2919	2437.8	0.7
Maintenance	3	2919	1693	1062.3	1.0
Maintenance	4	1693	45	2681.8	0.5

Table 5.1: *Parameter values for the production rates of the depletion field and the maintenance field.*

Field	Capacity (Sm3/d)	End of epoch (Days)
Depletion	1395	230
Maintenance	5525	180

Table 5.2: *Parameter values for the field capacities of the depletion field and the maintenance field. In both cases the epoch considered starts at production start.*

Field	Minimum regularity	Maximum regularity	Correlation factor ρ
Depletion	0.95	1.0	0.8
Maintenance	0.95	1.0	0.8

Table 5.3: *Parameter values for the regularity parameters of the depletion field and the maintenance field.*

	Disc. Prod.
Symmetry constraints	6,656.7
Priority constraints	6,678.9
Constant (1800, 700 Sm3/d)	6,594.3
Constant (2058, 442 Sm3/d)	6,657.5

Table 5.4: *Discounted production values (KSm3) for the different strategies.*

6 Conclusions

In the present paper we have demonstrated that production profile models based on hybrid systems are both fast and flexible. Thus, this approach is particulary useful in the context of total value

	Net Present Value
Symmetry constraints	2,303
Priority constraints	2,310
Constant (1800, 700 Sm3/d)	2,281
Constant (2058, 442 Sm3/d)	2,303

Table 5.5: *Net present values in* $1,000,000$ *USD for the different strategies.*

Oil price in USD per barrel						
20	30	40	50	60	70	80
2,692	4,038	5,384	6,730	8,075	9,421	10,767

Table 5.6: *Difference in net present value in* $1,000$ *USD between priority constraints and optimized quota constraints for different choices of oil price.*

chain analysis of large-scale development projects. Hybrid systems allow us to model multisegment production profiles, foreseen and unforeseen delays in production, as well as multiple production profiles. Furthermore, this paper has studied different allocation strategies for subfields with common capacity constraints.

A natural next step is to optimize these allocation strategies. The inclusion of uncertainty in the analysis of multiple production profiles with common capacity constraints is also an important issue that needs to be treated and studied. Furthermore, it is also important to incorporate gas and water production into the model framework. As a consequence the complexity of the model will increase and the transparency may decrease. Bearing in mind that parsimonious modeling is a virtue these consequences are not desired. All the same we believe it is of great value to be able to incorporate gas and water production into the framework since these aspects are essential in the context of a total value chain analysis.

Finally, the framework can be used to analyze a wide range problems that arise in the context of total value chain analysis. Such problems could include crucial investment decisions regarding infrastructure on the platform, i.e. capital expenditure decisions. Another problem that could be of interest to analyze is the economic effect of different production plan schedules, such as the issue of phasing in and phasing out different subfields of a major field.

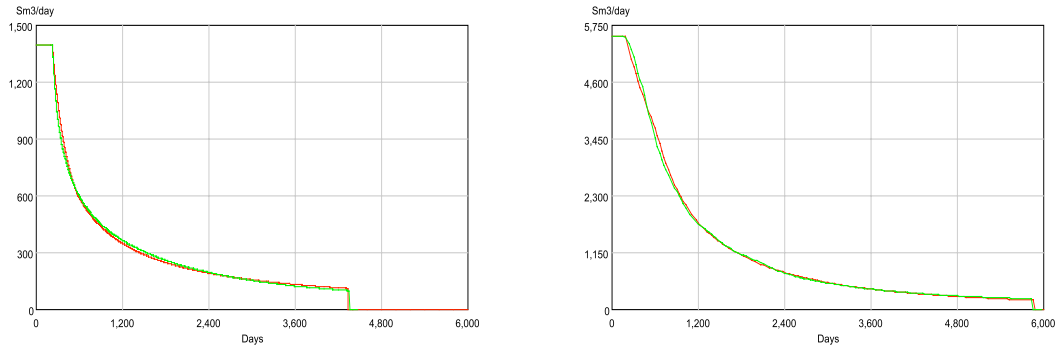

Figure 5.1: *The simulation profile and the matched profile comparison for the depletion field (left panel) and the maintenance field (right panel). In both panels the green curve represents the production rate from the simulation software, while the red curve represents the production rate from our model.*

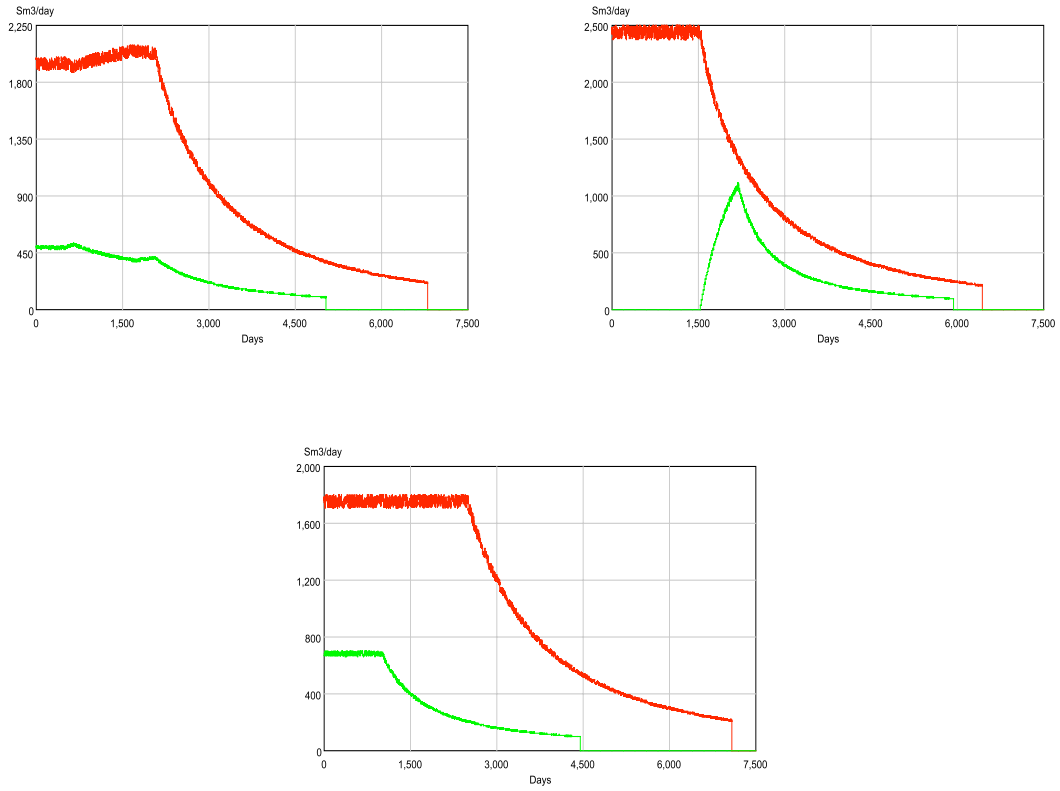

Figure 5.2: *The production rate of the depletion field (green graph) and the maintenance field (red graph) for different choices of constraints. The upper left panel illustrates continuous control with symmetry constraints. The upper right panel illustrates continuous control with priority constraints, where the maintenance field is being prioritized throughout the entire production period. The lower panel illustrates quota model with constant constraints. The maintenance field receives a constant quota of* $1800Sm3/day$ *while the depletion field receives a constant quota of* $700Sm3/day$*. In all panels the x-axis represents days and the y-axis represents Sm3/day.*

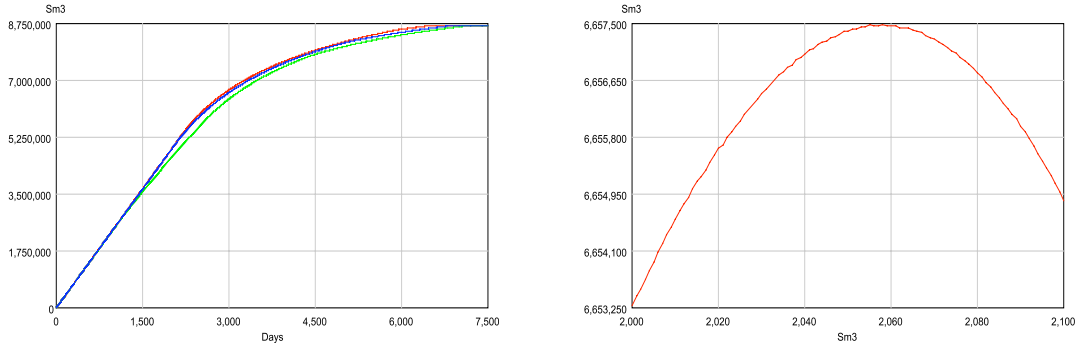

Figure 5.3: *The left panel illustrates total cumulative production for the three choices of constraints. Total cumulative production curves for priority constraints and symmetry constraints are illustrated by the red and blue graph, respectively. The green graph illustrates total cumulative production for the quota constraints model where the quota is* $1800Sm3/d$ *for the maintenance field and* $700Sm3/d$ *for the depletion field. The right panel illustrates discounted production as a function of the constant quota assigned to the maintenance field.*

7 Appendix: Solution to the Li-Horne Differential Equation

In this section we show how to solve the differential equation corresponding to the production model introduced in [7]. We denote the cumulative production function at time $t \geq t_0$ by $y(t)$. For given positive constants a and b, the Li-Horne differential equation can be written as:

$$\frac{dy}{dt} = a\frac{1}{y(t)} - b, \tag{7.1}$$

with the boundary condition that $y(t_0) = y_0$. Note first that if $y_0 = 0$, the derivative is undefined for $t = t_0$. Thus, we assume that $y_0 > 0$.

Before we solve the equation, we verify the existence and uniqueness of a solution by showing that the equation satisfies the well-known *Lipschitz condition*. In order to do so, we introduce the function $f = f(t, y)$, defined as:

$$f(t, y) = a\frac{1}{y(t)} - b. \tag{7.2}$$

We claim that f is Lipschitz on the set $R = \{(t, y) : t \geq t_0, y \geq y_0\}$. That is, for all $t \geq t_0$ and $y_1, y_2 \geq y_0$, there exists a K such that:

$$|f(t, y_1) - f(t, y_2)| \leq K|y_1 - y_2|. \tag{7.3}$$

This follows since:

$$|f(t, y_1) - f(t, y_2)| = a|\frac{1}{y_1} - \frac{1}{y_2}| = \frac{a}{y_1 y_2}|y_1 - y_2| \leq \frac{a}{y_0^2}|y_1 - y_2|. \tag{7.4}$$

In order to solve the differential equation (7.1), we multiply both sides of the equation by $y(t)dt$ and rewrite it in the following *differential* form:

$$(\frac{a}{b} - y)dt - \frac{y}{b}dy = 0. \tag{7.5}$$

This equation can be reduced to an exact differential equation by multiplying by a suitable integrating factor, $Q(t, y)$. (See e.g., [3] for details about this technique.) It turns out that the following function can be used for this purpose:

$$Q(t, y) = \exp(\frac{b^2}{a}t + \frac{b}{a}y). \tag{7.6}$$

After multiplying the equation by $Q(t, y)$, the equation can be written in the following form:

$$M(t, y)dt + N(t, y)dy = 0, \tag{7.7}$$

where:

$$\begin{aligned} M(t, y) &= (\frac{a}{b} - y)\exp(\frac{b^2}{a}t + \frac{b}{a}y), \\ N(t, y) &= -\frac{1}{b}y\exp(\frac{b^2}{a}t + \frac{b}{a}y). \end{aligned} \tag{7.8}$$

It is easy to verify that M and N satisfy the requirement for an exact differential. Specifically, we get that:

$$\frac{\partial M}{\partial y} = \frac{\partial N}{\partial t} = -\frac{b}{a}y\exp(\frac{b^2}{a}t + \frac{b}{a}y). \tag{7.9}$$

We then proceed by looking for a function $F(t, y)$ such that:

$$\begin{aligned} \frac{\partial F}{\partial t} &= M(t, y), \\ \frac{\partial F}{\partial y} &= N(t, y). \end{aligned} \tag{7.10}$$

By (7.8) F must satisfy:

$$F(t,y) = \int M(t,y)dt = (\frac{a}{b^2})(\frac{a}{b} - y)\exp(\frac{b^2}{a}t + \frac{b}{a}y) + \phi(y), \tag{7.11}$$

for some suitable function ϕ. By differentiating the expression (7.11) with respect to y and comparing the result to $N(t,y)$, it follows that ϕ must be a constant. Hence, the equation linking t and y must have the following form:

$$(\frac{a}{b^2})(\frac{a}{b} - y)\exp(\frac{b^2}{a}t + \frac{b}{a}y) = C, \tag{7.12}$$

for some constant C, or equivalently:

$$(\frac{a}{b} - y)\exp(\frac{b^2}{a}t + \frac{b}{a}y) = D, \tag{7.13}$$

for some constant D. Using the boundary condition $y(t_0) = y_0$, we get that D is given by:

$$D = (\frac{a}{b} - y_0)\exp(\frac{b^2}{a}t_0 + \frac{b}{a}y_0). \tag{7.14}$$

By inserting (7.14) into (7.13), we get the following relation between t and y:

$$\frac{\frac{a}{b} - y}{\frac{a}{b} - y_0}\exp(\frac{b}{a}(y - y_0)) = \exp(-\frac{b^2}{a}(t - t_0)). \tag{7.15}$$

Acknowledgments

This paper was written with support from the Norwegian Research Council as a part of the project STAR (grant number 154079) and Johan and Mimi Wesmann's foundation. The authors would like to thank Professor Eivind Damsleth, Chief Research Scientist Xeni Dimakos, Upstream Consulting Manager Steinar Lyngroth and Senior Risk Analyst Jingzhen Xu for many helpful comments and suggestions. We would also like to thank IPRES Consulting for introducing us to relevant business problems. The main parts of this paper were written during a sabbatical at Department of Electrical Engineering and Computer Sciences, at University of California, Berkeley. We are grateful to Professor Edward A. Lee and his group for hosting this sabbatical, and for introducing us to the field of hybrid systems.

References

[1] J. J. Arps. Analysis of decline curves. *Trans. AIME*, 160:228–247, 1945.

[2] R. Camacho and R. Raghavan. Boundary-dominated flow in solution-gas drive reservoirs. *SPERE*, pages 503–512, November 1989.

[3] J. W. Dettman. *Introduction to Linear Algebra and Differential Equations*. Dover, 1986.

[4] A. Gelman, J. B. Carlin, H. S. Stern, and D. B. Rubin. *Bayesian Data Analysis*. Chapman & Hall, 1995.

[5] A. B. Huseby and E. Brækken. An integrated risk model for reservoir and operational costs with application to total value chain optimization. *SPE*, (65145), 2000. Presented at the SPE European Petroleum Conference, Paris, France.

[6] P. E. Kloeden, E. Platen, and H. Schurtz. *Numerical Solutions of SDE Through Computer Experiments*. Springer–Verlag, Berlin–Heidelberg–New York, 2003.

[7] K. Li and R. N. Horne. A general scaling method for spontaneous imbibition. *SPE*, (77544), 2002. Presented at the SPE Annual Technical Conference, San Antonio, Texas.

[8] K. Li and R. N. Horne. A decline curve analysis model based on fluid flow mechanisms. *SPE*, (83470), 2003. Presented at the SPE/AAPG Western Regional Meeting, Long Beach, California.

[9] K. Li and R. N. Horne. Verification of decline curve analysis models for production prediction. *SPE*, (93878), 2005. Presented at the SPE Western Regional Meeting, Irvine, California.

[10] D. Liberzon. *Switching in Systems and Control*. Birkhauser, 2003.

[11] N. Liu. *Automatic History Matching Of Geologic Facies*. PhD thesis, University Of Oklahoma, Graduate College, 2005.

[12] T. Marhaendrajana and T. A. Blasingame. Decline curve analysis using type curves – evaluation of well performance behavior in a multiwell reservoir system. *SPE*, (71517), 2001. Presented at the SPE Annual Technical Conference and Exhibition, New Orleans, Louisiana.